Quantum dynamics of a vibronically coupled linear chain using a surrogate Hamiltonian approach

Myeong H. Lee* and Alessandro Troisi

Department of Chemistry and Centre for Scientific Computing,

University of Warwick, Coventry CV4 7AL, UK

(Dated: May 27, 2016)

Abstract

Vibronic coupling between the electronic and vibrational degrees of freedom has been reported to play an important role in charge and exciton transport in organic photovoltaic materials, molecular aggregates and light-harvesting complexes. Explicitly accounting for effective vibrational modes rather than treating them as a thermal environment has been shown to be crucial to describe the effect of vibronic coupling. We present a methodology to study dissipative quantum dynamics of vibronically coupled systems based on a surrogate Hamiltonian approach, which is in principle not limited by Markov approximation or weak system-bath interaction, using a vibronic basis. We apply vibronic surrogate Hamiltonian method to a linear chain system and discuss how different types of relaxation process, intramolecular vibrational relaxation and intermolecular vibronic relaxation, influence population dynamics of dissipative vibronic systems.

I. INTRODUCTION

Understanding the mechanism of charge and excitation-energy transfer in organic materials and light harvesting complexes has been the focus of many experimental and theoretical studies over the last few decades. In such photophysical processes there is often strong mixing between the electronic and vibrational degrees of freedom (DOF) and the vibronic coupling between the electronic and nuclear DOFs can play a significant role.[1–16] It has been reported that vibronic coupling is the origin of long-lived oscillations observed in two dimensional (2D) electronic spectra of the light-harvesting Fenna-Matthews-Olson (FMO) complex,[1–3] the photosystem II reaction centre,[4,5] an artificial molecular light harvester,[6] and a homodimer system.[7] Electronic resonance with vibrations has been suggested to enhance efficient photosynthetic energy transfer[10,17,18] and charge separation rate in oxygenic photosynthesis.[5] Evidence of the importance of vibronic coupling in ultrafast singlet fission has been recently provided by the experiments of ultrafast vibronic spectroscopy on thin films of TIPS-pentacene[11] and 2D electronic spectroscopy on pentacene and its derivatives[12] and by the computational studies.[13,14] Vibronic coupling was also suggested as an underlying mechanism for ultrafast coherent charge transfer in organic photovoltaic (OPV) heterojunctions using a combined approach of high time-resolution pump-probe spectroscopy and time-dependent density functional theory (TDDFT) simulations[15] and by quantum dynamics simulations.[16]

There have been considerable theoretical efforts to elucidate the role of vibrational DOF in the dynamics of charge and exciton transport.[1,3,16,17,19–26] It has been shown that explicitly accounting for effective vibrational DOFs (vibronic model) rather than incorporating them into the thermal reservoir (electronic model) can predict the system dynamics in better agreement with the experiment.[1,17,23] Christensson et al.[1] predicted the long-lived oscillations in the 2D spectra of the FMO complex with dephasing times that agree with the experimental results using a vibronic model, whereas the electronic model predicts a much faster time scale by an order of magnitude. Using a vibronic model Womick and Moran[17] explained the different relaxation rates observed in two cyanobacterial light-harvesting proteins despite the almost identical structures of their pigment dimers whereas the opposite trend was predicted using the electronic model.

In recent years quantum dynamics calculations based on a vibronic Hamiltonian have

been carried out for a variety of systems to study photoinduced dynamics at a conical intersection,[21,22] exciton dynamics and 2D spectra of a dimer system,[23,24,27,28] the effect of vibronic coupling on coherences and relaxation mechanisms in light-harvesting complexes,[1,2,17] and ultrafast charge transfer at the donor-acceptor interface of OPV heterojunctions.[16] Works based on Redfield theory[29–31] assume that the system-bath coupling is weak (to allow a perturbative treatment) and that the time scale of the bath dynamics is much faster than that of the system dynamics (to ignore memory effects and adopt the Markov approximation). However, the Markov approximation can be problematic when system dynamics occurs on ultrafast time scales and therefore the vibrational relaxation cannot be separated from the electronic relaxation. A modified Redfield theory[32,33] has been developed to go beyond weak system-bath coupling and applied to model the effect of vibronic coupling on the electronic relaxation rates in light-harvesting proteins.[17] The hierarchy equations of motion (HEOM)[34–43] method provides a computationally expensive, yet accurate way to model open quantum systems beyond the Markovian and perturbative approximations by introducing a set of auxiliary density operators. In recent years, the multi-configuration time-dependent Hartree (MCTDH) method,[44–46] where the multidimensional vibrational wavefunctions are described as a linear combination of the Hartree products of single-mode wave functions, has been used to describe e.g., the role of vibronic coupling in ultrafast charge transfer dynamics at an OPV donor-acceptor heterojunction.[16]

The surrogate Hamiltonian method[47–49] provides another means to study dissipative quantum dynamics without assuming a weak system-bath coupling or Markov approximation and has been shown to successfully model quantum dynamics of a variety of physical processes.[47,48,50–58] The basic idea of the surrogate Hamiltonian approach is to construct a *finite* system-bath Hamiltonian, which can reproduce the true system dynamics in the limit of an infinite number of bath modes for a finite time interval, by using the representative bath modes that span the typical energy range of the system.[47,50] Truncation of the infinite number of bath modes into the finite representative modes limits the description of system dynamics to short time evolution and recurrence eventually appears. Still, the surrogate Hamiltonian approach is advantageous to describe the vibronic relaxation process due to its less restrictive assumption on system-bath interaction and relative time scale of system dynamics. In addition, the construction of the bath can be done in a more controllable way and system-bath interactions can be tailored to a particular physical process of interest as

described in the next section.

Surrogate Hamiltonian method has been used to model nuclear/electronic relaxation/dephasing in photoinduced processes such as pump-probe charge transfer, photodesorption, and hot injection, where the system wavefunction is described using a grid representation.[50–55] In order to model exciton and charge transport in *large* systems such as photosynthetic complexes, for which the grid propagation method can be numerically expensive,[56] eigen-(site-)basis set has been introduced in the surrogate Hamiltonian method.[56–58] In those studies only electronic states were accounted for in the primary system and vibrational states were included in the bath. Herein we employ surrogate Hamiltonian method on a *vibronic* basis where the effective vibrational mode is explicitly incorporated into the primary system. In addition to the numerical advantage of a vibronic-basis description over a grid representation, the former can be also more useful for the specific experimental problems where certain vibrational levels and their resonance/off-resonance with electronic states are of interest[12,59,60] and/or the effect of high-frequency vibrational mode is important.[7] The vibronic basis set[61] has been vastly used to describe absorption and emission spectra of molecular aggregates[62–65] using the Holstein Hamiltonian[66] to study singlet fission in linear chains of molecules[67] and to explain the role of vibronic coupling in light-harvesting complexes in combination with a (modified) Redfield theory.[1,17] Employing a vibronic basis within the framework of the surrogate Hamiltonian quantum dynamics method allows us not only to go beyond weak system-bath coupling interaction and Markov approximation but also to investigate in a systematic way different types of relaxation mechanism in a vibronic system as described in the next section.

In the remainder of this paper, after introducing the surrogate Hamitonian method for vibronic Hamiltonians (section II), we consider a minimal dimer model (section III A) and a vibronic one-dimensional chain as a model of the OPV donor-acceptor interface (section III B).

II. METHODOLOGY

A. Surrogate Hamiltonian method in a vibronic basis

The total Hamiltonian of the system embedded in a bath can be written as the sum of system, bath and system-bath interaction terms,

$$\hat{H} = \hat{H}_{\mathrm{S}} + \hat{H}_{\mathrm{B}} + \hat{H}_{\mathrm{SB}}, \tag{1}$$

where

$$\hat{H}_{\mathrm{S}} = \sum_{i,\mathbf{v}} \sum_{j,\mathbf{w}} H^{(\mathrm{S})}_{i\mathbf{v},j\mathbf{w}} |i,\mathbf{v}\rangle\langle j,\mathbf{w}| \tag{2}$$

$$\hat{H}_{\mathrm{B}} = \sum_{k} \varepsilon_k \hat{\sigma}_k^\dagger \hat{\sigma}_k \tag{3}$$

$$\hat{H}_{\mathrm{SB}} = \sum_{k} \sum_{i,\mathbf{v}} \sum_{j,\mathbf{w}} \mathcal{G}^{(k)}_{i\mathbf{v},j\mathbf{w}} (\hat{\sigma}_k^\dagger + \hat{\sigma}_k) |i,\mathbf{v}\rangle\langle j,\mathbf{w}|. \tag{4}$$

Here $|i,\mathbf{v}\rangle = |i; v_1 \cdots v_m \cdots\rangle$ is a vibronic state of the primary system, which represents the product state of an electronic state $|i\rangle$ localized on molecular site i and N vibrational states $|\mathbf{v}\rangle = |v_1 \cdots v_N\rangle$ each localized on one of the N sites.[68,69] We adopt the site basis (diabatic representation) instead of eigenstate basis to describe the electronic states because the former is more convenient to describe the model Hamiltonian when the system-bath interaction is local, which is typically the case in a disordered system such as polymer. It should be noted that the quantum dynamics can be studied in any basis once the model Hamiltonian is obtained (e.g., Schröter et al.[70] described dissipative dynamics of an excitonic heterodimer using both adiabatic and diabatic representations). We defer a detailed description of $H^{(\mathrm{S})}_{i\mathbf{v},j\mathbf{w}}$ to the next section. In the surrogate Hamiltonian approach the bath modes are described by a finite number of non-interacting two-level systems (a so-called spin bath) and therefore $\hat{\sigma}_k^\dagger/\hat{\sigma}_k$ is the creation/annihilation operator of the spin bath mode k with energy ε_k. The spin bath allows a particularly efficient wavefunction propagation in very large Hilbert spaces by using a bit-ordered spinor as detailed in ref.[71] Eq. 4 describes the most general form of system-bath interaction where $\mathcal{G}^{(k)}_{i\mathbf{v},j\mathbf{w}}$ represents the system-bath coupling strength of the mode k associated with the transition between two vibronic states $|i,\mathbf{v}\rangle$ and $|j,\mathbf{w}\rangle$ of the primary system.

The Hamiltonian above is extremely general and the only approximation with respect to the most standard system-bath Hamiltonian is that the bath is not a collection of harmonic

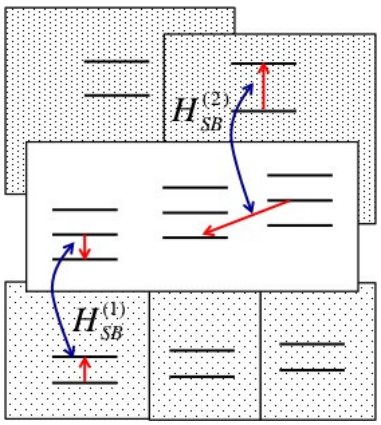

FIG. 1: Schematic of the system-bath interaction where the bath mode interacts locally with the vibronic states in its vicinity. Here $\hat{H}_{\rm SB}^{(1)}$ and $\hat{H}_{\rm SB}^{(2)}$ indicate the intramolecular and intermolecular system-bath interaction, respectively.

oscillators but spins. However, the spin bath can be considered an approximation of the harmonic oscillator at low bath temperature since no bath mode oscillator is highly excited at low temperature[47] and this analogy will be used to build models for realistic situations. (In fact, Gelman et al.[49] showed that the dynamics of the primary system of an anharmonic oscillator is not very different between the spin and harmonic baths except for extremely large system-bath coupling, which was carried out using the surrogate Hamiltonian approach and the MCTDH method, respectively.) In particular, the operator $\hat{\sigma}_k^\dagger + \hat{\sigma}_k$ is analogous to the displacement q_k of mode k. For the problems of exciton and charge transport we have a collection of electronic states localized in different regions of space, and nuclear modes of the system also localized in different regions. It is therefore appropriate to also assume that the bath modes $\{k\}$ are localized in such a way that each interacts only with a limited number of vibronic states in its vicinity (see Figure 1), which is different from the bath model employed in other surrogate Hamiltonian methods.[102]

B. 1D aggregates - The Primary system Hamiltonian

In this paper we consider for specificity the case of a one-dimensional (1D) aggregate of molecules with nearest neighbor interaction, a model that can be adapted to a number of interesting problems. Each molecular site is coupled to a single intramolecular vibrational mode with the frequency ω, whereas the remaining vibrational modes and the environmental

degrees of freedom are treated as a thermal bath. By considering a single electronic state per site, the vibronic system Hamiltonian can be written as[66,68,72,73]

$$\hat{H}_{\mathrm{S}} = \sum_i \sum_{\mathbf{v}} \big(E_i + n_{\mathbf{v}}\hbar\omega\big)|i,\mathbf{v}\rangle\langle i,\mathbf{v}| + \sum_i \sum_{\mathbf{v},\mathbf{w}} \Big[\tau V^{i,i+1}_{\mathbf{v},\mathbf{w}}|i,\mathbf{v}\rangle\langle i+1,\mathbf{w}| + \mathrm{H.c.}\Big]. \qquad (5)$$

The first term in eq. 5 represents the energy of a vibronic state $|i,\mathbf{v}\rangle$, where E_i is the electronic site energy and $n_{\mathbf{v}} = \sum_{m=1}^{N} v_m$ is the total vibrational quantum number with N being the number of molecules. (Here zero point energy is included in E_i and vibrational modes are assumed to be harmonic.) The second term represents the vibronic coupling, where τ is the electronic coupling (assumed to be the same for all adjacent pairs) and $V^{i,i+1}_{\mathbf{v},\mathbf{w}}$ is the vibrational coupling between two vibronic states $|i,\mathbf{v}\rangle$ and $|i+1,\mathbf{w}\rangle$,[67]

$$V^{i,i+1}_{\mathbf{v},\mathbf{w}} \;=\; \mathrm{FC}^{i,i+1}_{v_i,w_i}\,\mathrm{FC}^{i,i+1}_{v_{i+1},w_{i+1}} \prod_{m\neq i,i+1}^{N} \delta_{v_m,w_m}, \qquad (6)$$

where $\mathrm{FC}^{i,i+1}_{v_i,w_i}$ is the Franck-Condon factor, i.e., the overlap integral between the vibrational states $|v_i^i\rangle$ and $|w_i^{i+1}\rangle$ belonging to the electronic states $|i\rangle$ and $|i+1\rangle$, respectively. (Here $|v_i^i\rangle$ and $|v_{i+1}^i\rangle$ indicate the vibrational state localized on site i and $i+1$, respectively, belonging to the electronic state $|i\rangle$.) The Franck-Condon factor can be obtained via the analytical expression[31] once the Huang-Rhys factor S, which describes the electron-vibrational coupling strength, is determined.

C. 1D aggregates - form of the system-bath Hamiltonian

1. *Pure vibrational relaxation*

This is the transition between state $|i,\mathbf{v}\rangle$ and state $|i,\mathbf{w}\rangle$ differing by the vibrational quantum numbers. In analogy with conventional vibrational relaxation theory with a harmonic bath we allow transitions between states only differing by one vibrational quantum number (this would be the consequence of linear system-bath coupling in a harmonic bath). The energy difference between initial and final states will correspond to excitation/de-excitation of a bath mode. It is expected that different bath modes are responsible for the relaxation process in different portions of the system. Therefore, rather than using the index k for the modes we label them by the double index jk where j indicates the position where they are

located (between 1 and N) and k is a mode number index. (e.g., The mode jk promotes transitions involving the site j). Thus, $\hat{H}_{\mathrm{SB}}$ in eq. 4 takes the following form:

$$\hat{H}^{(1)}_{\mathrm{SB}} = \sum_{i,\mathbf{v}} \sum_{j} \Big[\sqrt{v_j+1} \big| i; v_1, \cdots, v_j, \cdots \big\rangle \big\langle i; v_1, \cdots, v_j+1, \cdots \big| + \sqrt{v_j} \big| i; v_1, \cdots, v_j, \cdots \big\rangle \big\langle i; v_1, \cdots, v_j-1, \cdots \big| \Big] \sum_k c_k \big(\hat{\sigma}^{\dagger}_{jk} + \hat{\sigma}_{jk} \big), \quad (7)$$

where c_k represents the strength of the interaction with mode k. In our model it does not depend on j because we are considering identical molecules. In section II D we discuss a suitable parameterization of c_k and the mode energy.

2. Intermolecular vibronic relaxation

This is the transition between two different vibronic states $|i, \mathbf{v}\rangle$ and $|j, \mathbf{w}\rangle$ ($i \neq j$), which can be considered as excitation energy transfer between pigment sites in the light harvesting complexes or charge relaxation between the molecular units in the organic solar cells. To express properly the Hamiltonian in the notation of the surrogate Hamiltonian we need to recall that electronic transitions are also promoted by nuclear modes (inducing modes) that modulate the electronic coupling between two states (Herzberg-Teller mechanism).[69,74–76] For instance, electronic transitions between localized states in polymeric semiconductors with (average) zero electronic coupling are promoted by inducing vibrational modes that modulate a coupling between two states. The strength of the intermolecular interaction is therefore also modulated by the Franck-Condon overlap between initial and final vibronic states. This component of the system-bath interaction takes the form:

$$\hat{H}^{(2)}_{\mathrm{SB}} = \sum_{i,\mathbf{v}} \sum_{\mathbf{w}} \big| i, \mathbf{v} \big\rangle \big\langle i+1, \mathbf{w} \big| V^{i,i+1}_{\mathbf{v},\mathbf{w}} \sum_k d_k \big(\hat{\sigma}^{\dagger}_{ik} + \hat{\sigma}_{ik} + \hat{\sigma}^{\dagger}_{i+1,k} + \hat{\sigma}_{i+1,k} \big) + \mathrm{H.}c. \quad (8)$$

We have assumed that the transition between the electronic states $|i\rangle$ and $|i+1\rangle$ is modulated by the modes localized in position i and $i+1$ in equal measure. The parameters d_k quantifying the strength of the interaction with the bath could in principle depend on i, but we assume here that there is translational symmetry in the inter-molecular aggregate. Here we neglect the coupling between the bath and electronic states that are not nearest neighbors and allow energy relaxation between all vibronic states as long as they belong to adjacent sites. (Eq. 8 can be easily modified to simulate a particular relaxation pathway of interest if necessary.)

It should be noted that the modulation of the site transition energy, associated with the transition between two different vibrational levels on the same molecular site, also promotes electronic transitions and it is accounted for in eq. 7.

Eqs. 7-8 take a slightly different form from the expression of the system-bath interaction for the electronic relaxation process typically found in literature,[56–58] where $\hat{H}_{\mathrm{SB}}$ is described as a tensor product of the system and bath operators (meaning that system and bath operators can be separated). In that case the system operator, which is independent of the bath mode, defines the relaxation pathway and each bath mode is involved in any transition equally. As we wish to study electronic states localized in different portions of space, we have set the model in a way to allow only certain modes to promote certain transitions, i.e., the bath spin operator acts selectively on each transition.

D. Parameterization of the system-bath Hamiltonian

The general strategy to parameterize the system-bath Hamiltonian is to assume a standard bath spectral density $J(\varepsilon)$. The system-bath coupling strength d_k in the surrogate Hamiltonian approach is given by[47,48,50]

$$d_k = \sqrt{\frac{J(\varepsilon_k)}{\rho(\varepsilon_k)}}, \tag{9}$$

where $\rho(\varepsilon_k) = [\varepsilon_{k+1} - \varepsilon_k]^{-1}$ corresponds to the density of bath modes. The bath spectral density $J(\varepsilon)$ is in general described as a continuous function of bath energy and determined by two parameters, the global system-bath coupling strength parameter λ and the characteristic time scale ε_c^{-1} of the bath correlation function (e.g., $J(\varepsilon) = 2\lambda\varepsilon\varepsilon_{\mathrm{c}}/(\varepsilon^2 + \varepsilon_{\mathrm{c}}^2)$ for the Drude-Lorentz spectral density).[77,78] Here the global system-bath coupling strength parameter λ is a measure of the off-diagonal electron-phonon coupling strength. For the simplest case of a homodimer system with $E_1 = E_2$, λ is the reorganization energy associated with the geometry relaxation due to the non-local electron phonon coupling. This type of bath spectral density can be used to describe d_k for the intermolecular vibronic relaxation in eq. 8, where relaxation energies are not uniform across transitions.

However, for the specific problem of purely vibrational relaxation (eq. 7) all transitions involve the same energy difference (this is a consequence of having harmonic nuclear modes). Therefore, it is more efficient to employ a bath model with a discrete spectral density,

described by a δ-function, with bath mode energies distributed around the vibrational transition energy $\hbar\omega$. Here we set the system-bath coupling strength independent of mode k, i.e., $c_k = c$.

E. Numerical approximation and wavefunction propagation

The forms chosen for the system-bath coupling are physically justified and chosen to be dependent on a very small number of parameters. These are not critical approximations in the sense that one can consider more general forms for the system-bath coupling without adding much additional cost to the calculation. The critical approximations discussed in this section are (i) setting a finite size of the system space and (ii) setting a finite size of the bath space. These approximations are to reduce the computational cost without altering the outcome significantly. For any problem of interest one needs to verify that the observables are converged with respect to the increase of both sizes.

The dimension of the system Hilbert space increases exponentially with the number of molecular sites, given by $N \times L^N$ for a 1D chain model with N sites and L vibrational levels per site. However, it may not be necessary to consider all possible vibronic states because vibronic states with a large quantum number are not likely to play an important role in overall system dynamics. Therefore, we introduce a scheme to restrict the number of vibronic states $\{|i, v_1 \cdots v_m \cdots\rangle\}$ included in the system Hamiltonian (eq. 5). As we will consider problems where the on-site electronic energy can be different, we consider a set of vibronic states such that $E_i + n_{\mathbf{v}}\hbar\omega \leq E_{\text{cutoff}}$. In this way a smaller number of vibrational states are included when the electronic energy is higher.

The spin bath state with M bath modes is described by a 2^M dimensional spinor and its dimensionality increases rapidly with M. It has been shown that it is not necessary to consider all possibilities of the bath mode excitations when the system-bath coupling is weak and therefore the number of simultaneous excitations can be restricted (to a single phonon excitation for the extreme case).[47,49,50,52] When the number of simultaneous excitations is restricted to N_{exc}, the dimension of the bath spinor is reduced to $\sum_{k=0}^{N_{\text{exc}}} \binom{M}{k}$, where $\binom{M}{k} = \frac{M!}{k!(M-k)!}$ denotes the binomial coefficients.

We assume that the system-bath states are not correlated at t=0, which is likely to be the case, e.g., upon photoexcitation. We set the bath temperature to 0 K and therefore do

not consider the random phase factor when constructing the initial bath state. Then, the initial total wavefunction can be simply given by the tensor product of the initial system wavefunction and the bath ground state wavefunction where no bath mode is excited. The initial wavefunction for the total system $|\psi(0)\rangle$ is propagated by applying the time evolution operator, $|\psi(t)\rangle = e^{-i\hat{H}t/\hbar}|\psi(0)\rangle$, which is done by expanding the time evolution operator by a series of Chebychev polynomials.[79–81] Once the quantum dynamics of the total wavefunction is obtained, the temporal evolution of the system observables can be evaluated from the reduced density operator $\hat{\rho}_{\rm S}(t)$ obtained by tracing out the bath modes from the total density operator

$$\hat{\rho}_{\rm S}(t) = {\rm Tr}_{\rm B}\{\hat{\rho}(t)\} = \sum_b \langle b|\psi(t)\rangle\langle\psi(t)|b\rangle, \tag{10}$$

where $|b\rangle$ is the bath eigenstate and ${\rm Tr}_{\rm B}\{\ \}$ denotes a partial trace over the bath states.

III. APPLICATIONS

A. Dimer system

A vibronic dimer is highly relevant to the study of exciton transfer in light harvesting complexes and molecular aggregates[3,9,17,23] and has been extensively used to obtain experimental observables such as 2D electronic/vibronic spectra[2,10,25,27,28,82–85] and absorption/fluorescence spectra.[18,86] We consider a single electronic state per molecular site. The system parameters are set to $\Delta E_{12} = E_2 - E_1$=1274 cm^{-1} (=0.158 eV), τ=81 cm^{-1} (=0.01 eV), ω=1400 cm^{-1} ($\hbar\omega$=0.174 eV), and Huang-Rhys factor S=0.5. (The same parameter values of τ, ω, and S are used in section III B unless noted otherwise.) To simplify the analysis, the maximum vibrational quantum number L_i of each electronic state $|i\rangle$ is set to L_1=1 and L_2=0. At t=0 the wavefunction is localized on the molecular site i=2 in the vibrational ground state, i.e., $|\psi(t=0)\rangle = |2;00\rangle$. The number of simultaneous excitations of the bath modes is limited to $N_{\rm exc}$=2 in all cases. (We found that a further increase of $N_{\rm exc}$ does not alter the system dynamics.)

1. Intramolecular vibrational relaxation

We first consider the case where only intramolecular vibrational relaxation occurs ($\hat{H}_{\rm SB}^{(1)} \neq 0$, $\hat{H}_{\rm SB}^{(2)} = 0$). We set the number of bath modes coupled to each site to M_1=9 and M_2=0 since L_2=0. (We obtain the same population dynamics by setting M_2=9.) This illustrates the advantage of employing bath modes localized in space, by having the flexibility of using different qualities of bath description on different sites. The bath modes are constructed with constant energy spacing $\delta\varepsilon$=32 cm^{-1}, centered at $\hbar\omega$. (Further details on construction of the bath modes can be found in section I in supplementary material (SM).)

The time evolution of the population of site 2 is plotted in Figure 2a for different values of the system-bath coupling strength c. (The population of site i is computed by $P_i(t) = \sum_{\mathbf{v}} \langle i, \mathbf{v}|\hat{\rho}_{\rm S}(t)|i, \mathbf{v}\rangle$.) The initial decay rate of the population (t<0.1 ps) is almost identical in all cases because any significant effect of the dissipative environment does not take place in this short time scale. Without the coupling to the bath (c=0), the population dynamics exhibits a Rabi-type coherent oscillation. This coherent oscillation has vibronic nature with most contribution coming from the vibrational excited state of site 1 ($|1;10\rangle$) and the vibrational ground state of site 2 ($|2;00\rangle$), due to their close energy level alignment. The coupling to the bath leads to a damped oscillation of the population. As c increases, the population of site 2 decays rapidly and vibronic coherent oscillatory features become strongly suppressed with time. We also find high-frequency oscillatory features with very small amplitude, which originate from the transitions between the $|2;00\rangle$ and $|1;00\rangle$ states. (See section IIA and Figure S2 in SM for Fourier analysis of the population to identify the origin of the oscillations). These electronic coherences are more pronounced after the initial decay (t>0.1 ps) and are preserved almost independently of the system-bath coupling strength c. To assure the assignment of the observed coherences we plot the real and imaginary parts of the coherences between each pair of the vibronic states in Figure 2b. (The coherence between vibronic states $|i, \mathbf{v}\rangle$ and $|j, \mathbf{w}\rangle$ is computed by $C_{i\mathbf{v},j\mathbf{w}}(t) = \langle i, \mathbf{v}|\hat{\rho}_{\rm S}(t)|j, \mathbf{w}\rangle$.) As expected, the vibronic coherences $C_{(1;10),(2;00)}$ are dominant over the electronic coherences $C_{(1;00),(2;00)}$. Our results indicate that the vibronic surrogate Hamiltonian method can differentiate between electronic and vibronic coherences, which is critical to understand the underlying mechanisms of efficient charge and exciton transport.

Figure 2a also demonstrates how the bath mode energy (or bath spectral density) influ-

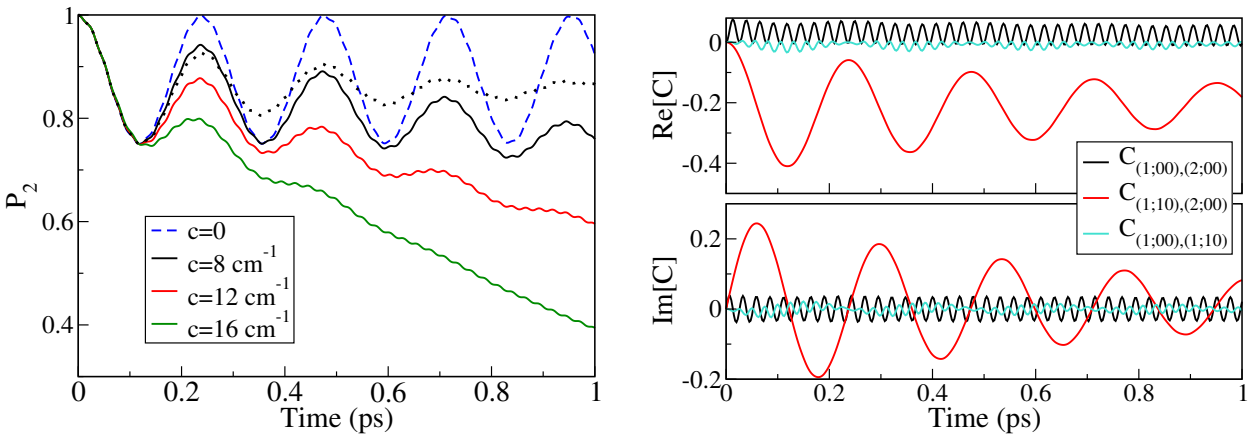

(a) (b)

FIG. 2: Intramolecular vibrational relaxation of a dimer. (a) Time evolution of the population of site 2 with varying c for $\delta\varepsilon$=32 cm^{-1} (dotted line indicates $P_2(t)$ for $\delta\varepsilon$=16 cm^{-1} and c=8 cm^{-1}). (b) Real and imaginary parts of coherence $C_{i\mathbf{v},j\mathbf{w}}$ for c=8 cm^{-1}. The vibronic coherence $C_{(1;10),(2;00)}$ is largest and $C_{(1;00),(1;10)}$ is almost negligible.

ences population dynamics. In the figure, $P_2(t)$ for $\delta\varepsilon$=16 cm^{-1} (black dotted line) fluctuates around 0.86, whereas it continues to decay for $\delta\varepsilon$=32 cm^{-1}. Efficient population relaxation for the latter results from the close energy-level alignment of the bath modes to the inter-site transition energy. (The energy levels are off by 5.6 and 0.56 cm^{-1} for $\delta\varepsilon$=16 and 32 cm^{-1}, respectively.) Very different population relaxation dynamics depending on the construction of the bath spectral density suggests that some of the phenomenology can be described poorly by a bath that is incorrectly parameterized, i.e., the description of open quantum dynamics in vibronic systems may need to be supported by good computational studies to determine system-specific parameters. This sensitive behavior also indicates another possibility of controlling system dynamics by modulating the system-bath interaction, which is in line with the previous studies,[56,87] in addition to controlling it by an external field.[88]

2. *Vibronic relaxation*

In this section we first consider the case where the relaxation mechanism is entirely governed by the intermolecular vibronic relaxation ($\hat{H}^{(1)}_{\rm SB}$ =0, $\hat{H}^{(2)}_{\rm SB}$ ≠0) and then discuss the more general case where both intramolecular and intermolecular relaxation pathways coexist ($\hat{H}^{(1)}_{\rm SB}$ ≠0, $\hat{H}^{(2)}_{\rm SB}$ ≠0). To model intermolecular relaxation we employ the Drude-Lorentz bath

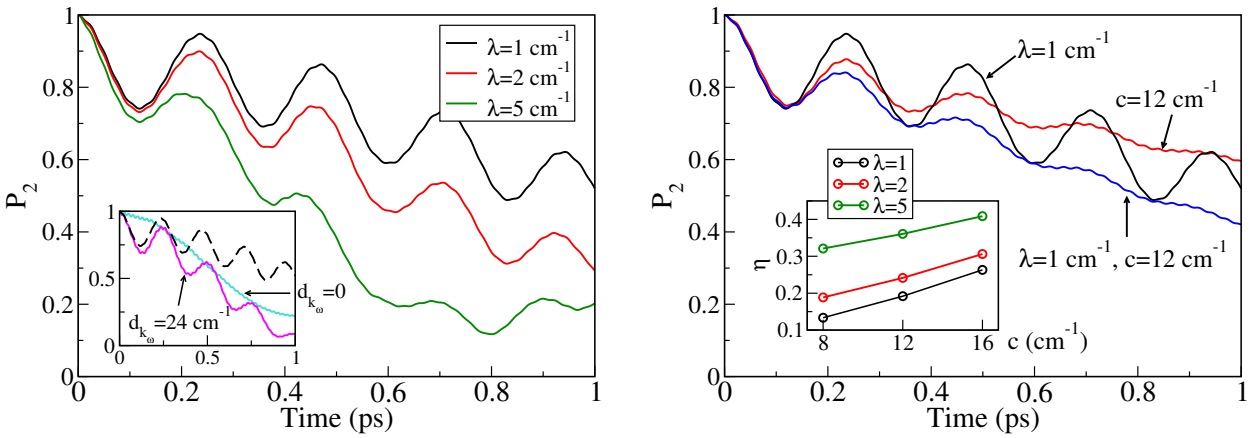

(a) (b)

FIG. 3: Population dynamics of site 2 of a dimer. (a) Intermolecular vibronic relaxation with varying λ. Recurrences, which is an artifact of the method using the finite size of the bath, occur after $\sim$0.8 ps for λ=5 cm^{-1}, indicating the backflow of energy from the bath to the system. Inset shows $P_2(t)$ using an electronic basis (solid lines) compared to using a vibronic basis (dashed line). (b) $P_2(t)$ when both relaxation pathways are accessible (λ=1 cm^{-1}, c=12 cm^{-1}). Inset shows relaxation efficiency η with varying c and λ.

spectral density described in section II D with ε_c=106 cm^{-1}. Nine bath modes are coupled to *each* molecular site and total 27 bath modes are used to model both relaxation pathways. The time evolution of the population for purely intermolecular relaxation is plotted for different values of λ in Figure 3a. As we have seen for the intramolecular vibrational relaxation, the initial decay rate of the population (t<0.1 ps) is very similar regardless of the system-bath coupling strength λ because the initial population dynamics is mostly determined by the transition between the $|1;10\rangle$ and $|2;00\rangle$ states. In addition, the population dynamics exhibits coherent oscillations with a vibronic origin arising from the oscillation between the $|1;10\rangle$ and $|2;00\rangle$ states (see section IIB in SM for discussions on the nature of coherences in detail). As the λ increases, the population decay becomes stronger and the oscillatory feature becomes weaker.[103]

Next, we explore the difference between using an electronic basis and using a vibronic basis. For the electronic basis the bath has additional high-frequency intramolecular vibrational mode described by the δ-function spectral density with the system-bath coupling strength d_{k_ω}. (Note that d_{k_ω}=0 leads to the same bath used for a vibronic basis). Inset

in Figure 3a shows the population obtained using a vibronic basis (dashed line) and using an electronic basis (solid line) for two different values of d_{k_ω}. Electronic model with d_{k_ω}=0 leads to the population dynamics very different from that of the vibronic model, i.e., no vibronic oscillatory features are observed and the population decays with very different rates. On the other hand, the population of the electronic model with d_{k_ω}=24 cm^{-1} exhibits vibronic oscillatory features and decays with the rate similar to the vibronic model at t<0.1 ps, whereas the population starts to deviate from that of the vibronic model afterwards. Our results suggest that electronic model may be able to describe qualitative features of the system dynamics when high-frequency vibrational modes are explicitly accounted for in the bath, but the rate of population relaxation can be quite different from that of the vibronic model, which demonstrates the importance of treating effective vibrational modes explicitly in the primary system to model vibronically coupled systems.

Next, we consider the case where the system-bath interaction includes both intramolecular and intermolecular relaxation ($\hat{H}_{\mathrm{SB}} = \hat{H}^{(1)}_{\mathrm{SB}} + \hat{H}^{(2)}_{\mathrm{SB}}$). The time evolution of the population is plotted in Figure 3b for the parameters λ=1 cm^{-1} and c=12 cm^{-1}, where the population evolution for purely intramolecular vibrational relaxation (c=12 cm^{-1}) and for purely intermolecular vibronic relaxation (λ=1 cm^{-1}) is also plotted for comparison. The initial decay of the population (t<0.1 ps) is quite similar in all cases because time evolution of the population on this time scale is mostly determined by the non-dissipative quantum dynamics. Similarly to intramolecular vibrational relaxation, vibronic coherent features are almost lost after 1 ps when both relaxation pathways are accessible. In general, population evolution under both relaxation mechanisms is largely determined by the relative strength of the system-bath interaction of each relaxation mechanism (λ and c). One important measure of efficiency of population relaxation is how fast the ground state gains its population. We obtain the relaxation efficiency η by evaluating the accumulated population of the ground state over time before recurrence occurs: $\eta \equiv (1/\tau)\int_0^\tau dt \langle\psi_g|\hat{\rho}_S(t)|\psi_g\rangle$,[56,89] where $|\psi_g\rangle$ is the vibronic ground state ($|1;00\rangle$) and the time window of integration τ is set to 0.7 ps in all cases. We note in passing that η can be sensitive to the value of τ and therefore should be interpreted as only a qualitative measure of relaxation efficiency. As expected, η increases as the system-bath coupling strength c or λ increases (see inset in Figure 3b). It is also seen that η increases almost linearly with c for a given value of λ (η also exhibits a similar behavior with λ for a given value of c − figure not shown). This trend, however, should not

be generalized to cases where the relaxation pathway involves multiple target states.[56] It should also be noted that other bath parameters such as ε_c and $\delta\varepsilon$ may affect η. Note that generalization to a vibronic basis improves the fidelity to the real system, but also increases the number of parameters of the model.

B. A 1D model for charge relaxation in OPV cells

We consider a 1D vibronic chain with parameters chosen to describe the physics of charge relaxation in OPV donor-acceptor interfaces. The electronic energy levels are given by $E_i{=}-\frac{e^2}{4\pi\epsilon Di}$, where ϵ is the permittivity of the dielectric medium and D is the distance between adjacent sites. Such a system represents a good minimal model[90–93] for the process of charge generation/recombination in OPV cells. These states can be thought as those of an electron acceptor under the influence of a positive hole in the electron donor separated by a distance D from the nearest electron. One is particularly interested in the relaxation from a given energy level toward the lowest energy level E_1 because this is the process preliminary to the hole-electron recombination that technologists need to limit. As a minimal model to describe the charge relaxation process near the donor-acceptor interface, we consider a system of four acceptor sites. We set the initial wavefunction localized on the acceptor site 3 in the vibrational ground state ($|\psi(t{=}0)\rangle{=}|3;0000\rangle$). This initial state can be considered as a charge-transfer (CT) state with an intermediate electron-hole separation, which may evolve into a charge-separated state or relax to a lower-energy CT state before charge recombination occurs. In this work we focus on the charge relaxation process and the role of vibronic coupling in that process.

The system parameters are set to $D{=}13$ Å, which corresponds to the acceptor-acceptor distance for fullerene derivatives, and $\epsilon = 3.5\epsilon_0$, which is close to the reported experimental value for OPV materials.[94,95] (The electronic energies of the dimer system in section III A correspond to the Coulombic on-site energies E_1 and E_2 with the electronic parameters used here.) Since the electronic energies are site-dependent, we impose the energy threshold to limit the number of states in the primary system as described in section II E. Due to the large energy gap between the initial state and the vibrational excited states of site 2 ($\Delta E{=}976$ cm^{-1}) and relatively small vibronic coupling (32 cm^{-1}) it is not likely that the vibratoinal excited states of site 2 plays a role in the population dynamics. Therefore, we

set the energy cutoff to $E_{\text{cutoff}} = E_3 + 0.5\hbar\omega$ (see inset on the left in Figure 4a), which results in total eight vibronic states in the primary system. (Note that there are four degenerate vibrational excited states with energy $E_1 + \hbar\omega$.) The primary system Hamiltonian is very sparse, i.e., only 28% of $\hat{H}_{\text{S}}$ elements are non-zero. It should be noted that, however, all system states are coupled via the bath. The bath parameters are set to $\delta\varepsilon$=129 cm^{-1} and ε_c=106 cm^{-1}. Total 25 bath modes are employed and the maximum number of simultaneous excitations is set to N_{exc}=2.[104]

The time evolution of the population of each site is plotted in Figure 4a for c=16 cm^{-1} and λ=1 cm^{-1}, where the population dynamics of a closed system is also plotted in the figure inset. Initial population dynamics is governed by the transitions between the $|3;0000\rangle$ and $|4;0000\rangle$ states and the transitions between the $|3;0000\rangle$ and $|2;0000\rangle$ states, where the former has larger transition probability due to closer energy level alignment ($E_4 - E_3 = (E_3 - E_2)/2$). Therefore, when the system is not coupled to the bath, the population of site 2 is much smaller than that of site 4 and the population of site 1 is almost negligible (see inset in Figure 4a). As the system is coupled to the bath and the system-bath interaction takes effect (t>0.1 ps), the population transfers from site 3 to site 2 and to site 1. As the system-bath interaction becomes stronger, the population of site 1 increases faster as shown in Figure 4b, where the P_1 is plotted for different values of c (increasing from 8 to 48 cm^{-1}) with λ=1 cm^{-1} and for different values of λ (=0.5, 1, 2, 5 cm^{-1}) with c=16 cm^{-1}. More specifically, an increase of the intramolecular relaxation parameter c leads to a faster increase of P_1 but a slower increase of P_2. On the other hand, an increase of the intermolecular relaxation parameter λ leads to a faster increase of both P_1 and P_2 and a faster decrease of P_3 accordingly (figure not shown). Different relaxation pathways modulate the population of each site differently, but stronger system-bath interaction ultimately leads to a faster charge relaxation to the lowest-lying CT state for both relaxation pathways. It is generally accepted that the single most important loss mechanism in OPV cells is the charge recombination and one of the key objectives in the field is therefore to reduce the rate of charge recombination. We have seen in this study that the rate of forming bound hole-electon pairs (the last intermediate before irreversible charge recombination occurs) is controlled by the system-bath interaction. A strategy to increase the efficiency of OPV cells is therefore to make the energy dissipation process inefficient, e.g., by first identifying the modes that are responsible for the dissipation and then defining strategies for reducing their

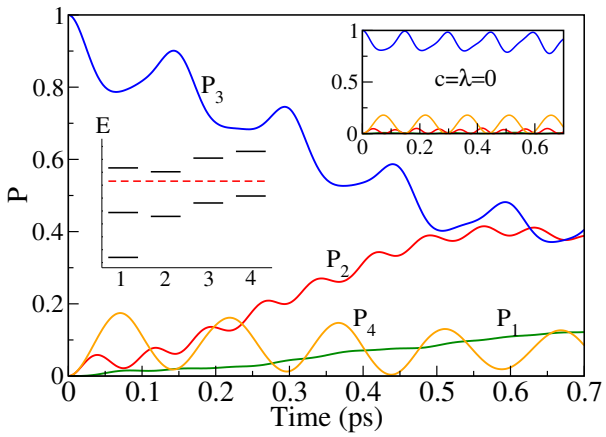

(a)

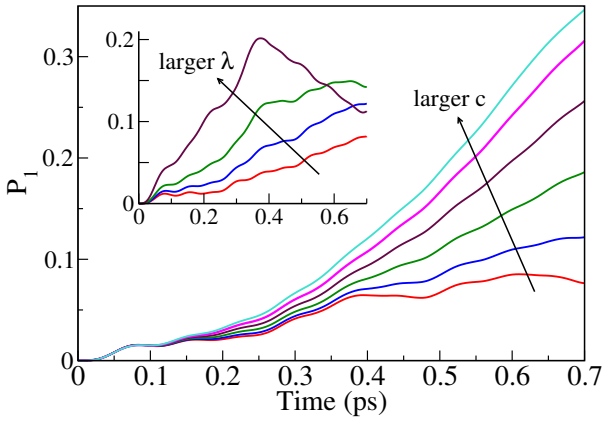

(b)

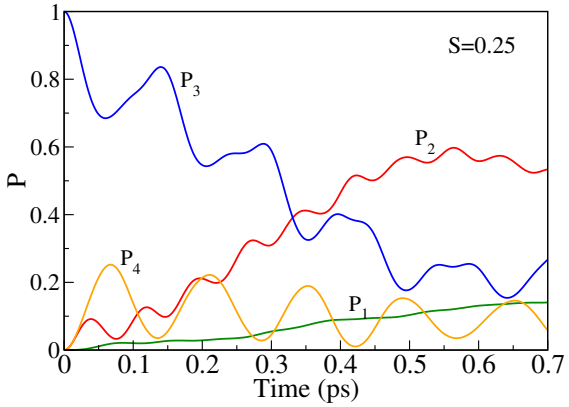

(c)

FIG. 4: Vibronic 1D chain (N=4) (a) Population of each site (P_i) for S=0.5. Inset on the top right corner shows $P_i(t)$ without coupling to the bath and inset on the left illustrates the energy levels with the cutoff energy (dashed line). (b) P_1 for different values of the system-bath coupling strength (c, λ). (c) Population of each site for S=0.25.

importance based on changing functional groups, controlling the interface energetics and morphology, etc. (Note the stark contrast between the qualitative features of this model and the kinetic Monte Carlo modeling of the same interface that assumes first order kinetic rate of hopping between sites with rates not depending on their energy difference.[96,97])

To see the importance of vibronic coupling in charge relaxation we obtain the population dynamics for different values of the Huang-Rhys factor S. It should be noted that the effect of S is more subtle because the Franck-Condon factor $\mathrm{FC}_{v,w}$ associated with the excited vibrational level, e.g., $\mathrm{FC}_{1,0}$ is not monotonic in S, whereas $\mathrm{FC}_{0,0}$ decreases with the increase of S. The most noticeable change, when the S is reduced from 0.5 (Figure 4a) to 0.25 (Figure 4c), is the increase of the population transition rate from site 3 to site 2 (and from site 3 to site 4) and the increase of the relaxation rate. We find the same trend, i.e., faster decay of the P_3 and faster rise of the P_2, when decreasing the S from 1 to 0.5, 0.25, and 0.1 (figure not shown). This can be explained by the increase of the coupling strength between sites 2 and 3 ($V^{2,3}_{(0000),(0000)}$) and between sites 3 and 4 ($V^{3,4}_{(0000),(0000)}$) as the S decreases (see eq. 6 and also note that the Franck-Condon factor $\mathrm{FC}^{i,i+1}_{v_i,w_i}$ for v_i=w_i=0 increases as the S decreases and here v_i=w_i=0 for sites i>1.) In addition, an increase of the vibrational coupling $V^{i,i+1}_{\mathbf{v},\mathbf{w}}$ leads to the increase of the intermolecular system-bath coupling strength (see eq. 8). On the other hand, the effect of the vibronic coupling strength on the population of site 1 appears as less significant for a given simulation time as compared to its effect on the P_2 or P_3. We find that the P_1 increases as the S increases from 0.1 to 0.25 but decreases as the S increases further to 0.5 and 1. A complete charge relaxation to the lowest-energy CT state, reaching an equilibrium, is expected to occur on tens of picoseconds to nanoseconds. The valid time scale of the simulation in this work is limited by the recurrence time (∼0.7 ps) resulting from the finite size of the bath. Nevertheless, our model demonstrates how charge relaxation dynamics is influenced by the vibronic coupling of the intramolecular vibrational mode to the electronic DOF.

IV. CONCLUSIONS

In this paper we presented a theoretical framework to model dissipative quantum dynamics of a vibronically coupled system using a vibronic basis and applied it to vibronic linear chain systems that can be related to realistic problems. To this end, the primary

system was assumed to be a 1D aggregate coupled to a single intramolecular vibrational mode with a single electronic state per site and nearest-neighbor electronic interaction, and the primary system Hamiltonian was constructed on a vibronic basis where the vibrational mode is explicitly accounted for. The system-bath interaction Hamiltonian was constructed to model the two main types of relaxation process, intramolecular vibrational relaxation and intermolecular vibronic relaxation, and different types of bath models were adopted for each relaxation process. Considering that the electronic states and nuclear modes in charge and exciton transport problems are localized in space, we employed a bath model with localized modes that interact with a limited number of states, which can be especially advantageous when only a limited number of molecular sites is actively involved in the system dynamics.

Our calculations suggest that the vibronic surrogate Hamiltonian approach can capture the effect of a dissipative environment on the dynamics of vibronically coupled systems and therefore provide a valuable tool to investigate the effect of vibronic coupling on charge and exciton transport in molecular systems. In addition, we have shown that the vibronic surrogate Hamiltonian method is able to identify the origin of coherences, whether they are vibronic or electronic. The surrogate Hamiltonian method employed in this work can be useful especially when the system dynamics occurs on ultrafast time scales or when the system-bath interaction cannot be assumed to be weak. Possible problems with suitable characteristics include exciton transport in photosynthetic complexes,[98] singlet fission[99] and charge separation of photogenerated excitons in OPV cells.[15,100,101] Our work can be extended in the future to provide a better description of the model Hamiltonian by employing parameters close to realistic molecular systems with the support of computational chemistry methods to obtain system-specific parameters.

SUPPLEMENTARY MATERIAL

See supplementary material for the vibrational relaxation of a monomer and coherence analysis of a dimer.

ACKNOWLEDGMENTS

This work was supported by ERC through Grant No. 615834. We thank Juan Aragó, Rocco Fornari, and Haibo Ma for carefully reading the manuscript and helpful comments.

* mail to: myeong.lee@warwick.ac.uk

[1] N. Christensson, H. F. Kauffmann, T. Pullerits, and T. Mančal, J. Phys. Chem. B **116**, 7449 (2012).

[2] C. Kreisbeck and T. Kramer, J. Phys. Chem. Lett. **3**, 2828 (2012).

[3] A. W. Chin, J. Prior, R. Rosenbach, F. Caycedo-Soler, S. F. Huelga, and M. B. Plenio, Nature Phys. **9**, 113 (2013).

[4] E. Romero, R. Augulis, V. I. Novoderezhkin, M. Ferretti, J. Thieme, D. Zigmantas, and R. van Grondelle, Nature Phys. **10**, 676 (2014).

[5] F. D. Fuller, J. Pan, A. Gelzinis, V. Butkus, S. S. Senlik, D. E. Wilcox, C. F. Yocum, L. Valkunas, D. Abramavicius, and J. P. Ogilvie, Nature Chem. **6**, 706 (2014).

[6] J. Lim, D. Paleček, F. Caycedo-Soler, C. N. Lincoln, J. Prior, H. von Berlepsch, S. F. Huelga, M. B. Plenio, D. Zigmantas, and J. Hauer, Nature Commun. **6**, 7755 (2015).

[7] A. Halpin, P. J. M. Johnson, R. Tempelaar, R. S. Murphy, J. Knoester, T. L. C. Jansen, and R. J. D. Miller, Nature Chem. **6**, 196 (2014).

[8] Y. Song, S. N. Clafton, R. D. Pensack, T. W. Kee, and G. D. Scholes, Nature Commun. **5**, 4933 (2014).

[9] E. J. O'Reilly and A. Olaya-Castro, Nature Commun. **5**, 3012 (2014).

[10] V. Tiwari, W. K. Peters, and D. M. Jonas, Proc. Natl. Acad. Sci. USA **110**, 1203 (2013).

[11] A. J. Musser, M. Liebel, C. Schnedermann, T. Wende, T. B. Kehoe, A. Rao, and P. Kukura, Nature Phys. **11**, 352 (2015).

[12] A. A. Bakulin, S. E. Morgan, T. B. Kehoe, M. W. B. Wilson, A. W. Chin, D. Zigmantas, D. Egorova, and A. Rao, Nature Chem. **8**, 16 (2015).

[13] S. Ito, T. Nagami, and M. Nakano, J. Phys. Chem. Lett. **6**, 4972 (2015).

[14] N. Renaud and F. C. Grozema, J. Phys. Chem. Lett. **6**, 360 (2015).

[15] S. M. Falke, C. A. Rozzi, D. Brida, M. Maiuri, M. Amato, E. Sommer, A. D. Sio, A. Rubio, G. Cerullo, E. Molinari, et al., Science **344**, 1001 (2014).

[16] H. Tamura, R. Martinazzo, M. Ruckenbauer, and I. Burghardt, J. Chem. Phys. **137**, 22A540 (2012).

[17] J. M. Womick and A. M. Moran, J. Phys. Chem. B **115**, 1347 (2011).

[18] A. Kolli, E. J. O'Reilly, G. D. Scholes, and A. Olaya-Castro, J. Chem. Phys. **137**, 174109 (2012).

[19] O. Kühn, T. Renger, and V. May, Chem. Phys. **204**, 99 (1996).

[20] R. Schneider, W. Domcke, and H. Köppel, J. Chem. Phys. **92**, 1045 (1990).

[21] A. Kühl and W. Domcke, J. Chem. Phys. **116**, 263 (2002).

[22] A. Kühl and W. Domcke, Chem. Phys. **259**, 227 (2000).

[23] S. Polyutov, O. Kühn, and T. Pullerits, Chem. Phys. **394**, 21 (2012).

[24] M. F. Gelin, L. Z. Sharp, D. Egorova, and W. Domcke, J. Chem. Phys. **136**, 034507 (2012).

[25] J. Seibt, K. Renziehausen, D. V. Voronine, and V. Engel, J. Chem. Phys. **130**, 134318 (2009).

[26] A. G. Dijkstra, C. Wang, J. Cao, and G. R. Fleming, J. Phys. Chem. Lett. **6**, 627 (2015).

[27] L. Z. Sharp and D. Egorova, J. Chem. Phys. **139**, 144304 (2013).

[28] V. Butkus, L. Valkunas, and D. Abramavicius, J. Chem. Phys. **140**, 034306 (2014).

[29] A. G. Redfield, IBM J. Res. Dev. **1**, 19 (1957).

[30] A. Nitzan, *Chemical Dynamics in Condensed Phases* (Oxford University Press, New York, 2006).

[31] V. May and O. Kühn, *Charge and Energy Transfer Dynamics in Molecular Systems* (Willey-VCH, Berlin, 2011), 3rd ed.

[32] W. M. Zhang, T. Meier, V. Chernyak, and S. Mukamel, J. Chem. Phys. **108**, 7763 (1998).

[33] M. Yang and G. R. Fleming, Chem. Phys. **275**, 355 (2002).

[34] J. Strümpfer and K. Schulten, J. Chem. Theory Comput. **8**, 2808 (2012).

[35] Y. Tanimura and R. Kubo, J. Phys. Soc. Japan **58**, 1199 (1989).

[36] Y. Tanimura, Phys. Rev. A **41**, 6676 (1990).

[37] Y. Tanimura, J. Phys. Soc. Japan **75**, 082001 (2006).

[38] C. Meier and D. J. Tannor, J. Chem. Phys. **111**, 3365 (1999).

[39] A. Pomyalov and D. J. Tannor, J. Chem. Phys. **123**, 204111 (2005).

[40] A. Pomyalov, C. Meier, and D. J. Tannor, Chem. Phys. **370**, 98 (2010).

[41] A. Ishizaki and Y. Tanimura, J. Phys. Soc. Japan **74**, 3131 (2005).

[42] Y. Yan, F. Yang, Y. Liu, and J. Shao, Chem. Phys. Lett. **395**, 216 (2004).

[43] R.-X. Xu and Y. Yan, Phys. Rev. E **75**, 031107 (2007).

[44] M. H. Beck, A. Jäckle, G. Worth, and H.-D. Meyer, Phys. Reports **324**, 1 (2000).

[45] M. Nest and H.-D. Meyer, J. Phys. Chem. **119**, 24 (2003).

[46] I. Burghardt, M. Nest, and G. A. Worth, J. Chem. Phys. **119**, 5364 (2003).

[47] R. Baer and R. Kosloff, J. Chem. Phys. **106**, 8862 (1997).

[48] D. Gelman and R. Kosloff, Chem. Phys. Lett. **381**, 129 (2003).

[49] D. Gelman, C. P. Koch, and R. Kosloff, J. Chem. Phys. **121**, 661 (2004).

[50] C. P. Koch, T. Klüner, and R. Kosloff, J. Chem. Phys. **116**, 7983 (2002).

[51] C. P. Koch, T. Klüner, H.-J. Freund, and R. Kosloff, Phys. Rev. Lett. **90**, 117601 (2003).

[52] C. P. Koch, T. Klüner, H.-J. Freund, and R. Kosloff, J. Chem. Phys. **119**, 1750 (2003).

[53] G. Katz, M. A. Ratner, and R. Kosloff, J. Phys. Chem. C **118**, 21798 (2014).

[54] G. Katz, M. A. Ratner, and R. Kosloff, J. Phys. Chem. A **115**, 5833 (2011).

[55] S. Dittrich, H.-J. Freund, C. P. Koch, R. Kosloff, and T. Klüner, J. Chem. Phys. **124**, 024702 (2006).

[56] N. Renaud, M. A. Ratner, and V. Mujica, J. Chem. Phys. **135**, 075102 (2011).

[57] N. Renaud, D. Powell, M. Zarea, B. Movaghar, M. R. Wasielewski, and M. A. Ratner, J. Phys. Chem. A **117**, 5899 (2013).

[58] N. Renaud, Y. A. Berlin, F. D. Lewis, and M. A. Ratner, J. Am. Chem. Soc. **135**, 3953 (2013).

[59] F. Novelli, A. Nazir, G. H. Richards, A. Roozbeh, K. E. Wilk, P. M. G. Curmi, and J. A. Davis, J. Phys. Chem. Lett. **6**, 4573 (2015).

[60] J. M. Womick, S. A. Miller, and A. M. Moran, J. Chem. Phys. **133**, 024507 (2010).

[61] M. R. Phipott, J. Chem. Phys. **55**, 2039 (1971).

[62] F. C. Spano, J. Chem. Phys. **116**, 5877 (2002).

[63] F. C. Spano, J. Chem. Phys. **122**, 234701 (2005).

[64] T.-S. Ahn, A. M. Müller, R. O. Al-Kaysi, F. C. Spano, J. E. Norton, D. Beljonne, J.-L. Brédas, and C. J. Bardeen, J. Chem. Phys. **128**, 054505 (2008).

[65] F. C. Spano, J. Clark, C. Silva, and R. H. Friend, J. Chem. Phys. **130**, 074904 (2009).

[66] T. Holstein, Ann. Phys. **8**, 325 (1959).

[67] F. Ambrosio and A. Troisi, J. Chem. Phys. **141**, 204703 (2014).

[68] A. Troisi, Phys. Rev. B **82**, 245202 (2010).

[69] R. P. Fornari, J. Aragó, and A. Troisi, J. Chem. Phys. **142**, 184105 (2015).

[70] M. Schröter, T. Pullerits, and O. Kühn, Ann. Phys. (Berlin) **527**, 536 (2015).

[71] C. Koch, Ph.D. thesis, Humboldt-Universität zu Berlin (2002).

[72] A. S. Alexandrov and J. Devreese, *Advances in Polaron Physics* (Springer, Heidelberg, 2010).

[73] A. S. Alexandrov, *Polarons in Advanced Materials* (Springer, Bristol, 2007).

[74] G. Herzberg and E. Teller, Z. Phys. Chem. B **21**, 410 (1933).

[75] H. J. Kupka, *Transitions in Molecular Systems* (Wiley-VCH, Weinheim, 2010).

[76] A. Troisi, A. Nitzan, and M. A. Ratner, J. Chem. Phys. **119**, 5782 (2003).

[77] S. Mukamel, *Principles of Nonlinear Optical Spectroscopy* (Oxford, New York, 1995).

[78] A. Kell, X. Feng, M. Reppert, and R. Jankowiak, J. Phys. Chem. B **117**, 7317 (2013).

[79] H. Tal-Ezer and R. Kosloff, J. Chem. Phys. **81**, 3967 (1984).

[80] R. Kosloff, Annu. Rev. Phys. Chem. **45**, 145 (1994).

[81] C. Leforestier, R. H. Bisseling, C. Cerjan, M. D. Feit, R. Friesner, A. Guldberg, A. Hammerich, G. Jolicard, W. Karrlein, H.-D. Meyer, et al., J. Comput. Phys. **94**, 59 (1991).

[82] M. B. Plenio, J. Almeida, and S. F. Huelga, J. Chem. Phys. **139**, 235102 (2013).

[83] F. Caycedo-Soler, A. W. Chin, J. Almeida, and S. F. Huelga, J. Chem. Phys. **136**, 155102 (2012).

[84] A. Chenu, N. Christensson, H. F. Kauffmann, and T. Mančal, Sci. Rep. **3**, 02029 (2013).

[85] V. Butkus, D. Zigmantas, D. Abramavicius, and L. Valkunas, Chem. Phys. Lett. **587**, 93 (2013).

[86] J. Schulze, M. Torbjörnsson, O. Kühn, and T. Pullerits, New J. Phys. **16**, 045010 (2014).

[87] A. Perdomo, L. Vogt, A. Najmaie, and A. Aspuru-Guzik, Appl. Phys. Lett. **96**, 093114 (2010).

[88] E. Asplund and T. Klüner, Phys. Rev. Lett. **106**, 140404 (2011).

[89] P. Rebentrost, R. Chakraborty, and A. Aspuru-Guzik, J. Chem. Phys. **131**, 184102 (2009).

[90] S. L. Smith and A. W. Chin, Phys. Chem. Chem. Phys. **16**, 20305 (2014).

[91] A. Troisi, Faraday Discuss. **163**, 377 (2013).

[92] H. Ma and A. Troisi, Adv. Mater. **26**, 6163 (2014).

[93] M. H. Lee, J. Aragó, and A. Troisi, J. Phys. Chem. C **119**, 14989 (2015).

[94] L. J. A. Koster, V. D. Mihailetchi, and P. W. M. Blom, Appl. Phys. Lett. **88**, 093511 (2006).

[95] A. J. Moulé and K. Meerholz, Appl. Phys. Lett. **91**, 061901 (2007).

[96] C. Groves, J. C. Blakesley, and N. C. Greenham, Nano Lett. **10**, 1063 (2010).

[97] T. M. Burke and M. D. McGehee, Adv. Mater. **26**, 1923 (2013).

[98] M. Sarovar, A. Ishizaki, G. R. Fleming, and K. B. Whaley, Nature Phys. **6**, 462 (2010).

[99] M. W. B. Wilson, A. Rao, J. Clark, R. S. S. Kumar, D. Brida, G. Cerullo, and R. H. Friend, J. Am. Chem. Soc. **133**, 11830 (2011).

[100] S. Gélinas, A. Rao, A. Kumar, S. L. Smith, A. W. Chin, J. Clark, T. S. van der Poll, G. C.

Bazan, and R. H. Friend, Science **343**, 512 (2014).

[101] A. E. Jailaubekov, A. P. Willard, J. R. Tritsch, W.-L. Chan, N. Sai, R. Gearba, L. G. Kaake, K. J. Williams, K. Leung, P. J. Rossky, et al., Nature Mater. **12**, 66 (2013).

[102] The localized basis is also convenient to ensure that the total Hamiltonian is size consistent, i.e., the bath and the system size can be increased in a consistent way if one needs to consider systems of different sizes.

[103] Increasing ε_c also leads to a slightly faster decay of the population due to an increase of $J(\varepsilon)$ at $\varepsilon = \Delta E_{12}$ as a result of the broadening of the bath spectral density and the shift of the peak position of the spectral density towards higher energy.

[104] The validity of setting N_{exc}=2 was tested for a dimer for each intramolecular and intermolecular relaxation pathway. We found that setting N_{exc} larger than 2 does not change the population dynamics at all.